Cryogenics 139 (2024) 103832

Contents lists available at ScienceDirect

Cryogenics

journal homepage: www.elsevier.com/locate/cryogenics

Investigations on the throttling process of ^3He in a dilution refrigerator used for cooling superconducting quantum chips

Shiguang Wu [a,c], Haizheng Dang [a,b,c,d,*]

[a] State Key Laboratory of Infrared Physics, Shanghai Institute of Technical Physics, Chinese Academy of Sciences, 500 Yutian Road, Shanghai 200083, China
[b] Shanghai Research Center for Quantum Sciences, Shanghai 201315, China
[c] University of Chinese Academy of Sciences, Beijing 100049, China
[d] Shanghai Boreas Cryogenics Co., Ltd, Shanghai 201802, China

ARTICLE INFO

Keywords:
Dilution refrigerator
Throttling process
^3He
Superconducting quantum chips
Quantum computing and communications

ABSTRACT

With the rapid progress of the superconducting quantum computing technology, the cryogenic technology capable of providing appropriate cooling in the millikelvin temperature region is desirable. The cryogen-free dilution refrigerator featuring high reliability, long lifetime, and continuous cooling has become one of the most promising cryocooler candidates for this purpose. As one of the key components of the dilution refrigerator, the impedance component is used to control the flow and to liquefy ^3He, which is crucial to achieving the millikelvin temperature. In this paper, a throttling model is proposed to analyze the dilution cycle and to eventually improve the refrigeration performance, which focuses on the influences of the complex physical properties of ^3He and the dilution cycle from the subcooled state to saturation state. The effects of the inlet pressure and inlet temperature on the flow rate are studied, and the energy conversion on the throttling process is discussed. It indicates that the throttling model can reasonably predict the flow rate under different inlet pressure and inlet temperature and is helpful to the design and optimization of the millikelvin cryogen-free dilution refrigerator.

1. Introduction

With the advancement of quantum computing [1] and quantum communications [2], there is a growing focus on dilution refrigerators employed to cool superconducting quantum chips [3]. The impedance component plays a crucial role in the cooling process through throttling and serves as a pivotal component within the dilution refrigerator.

In the research of dilution refrigerators, most scholars focus on the performance of the heat exchanger, with little attention given to the impact of the impedance component on the dilution refrigerator. Shang et al. [4] developed a heat exchanger model applicable within the millikelvin temperature range of a dilution refrigerator. The study delved into the impact of Kapitza thermal conductivity, axial thermal conductivity, and impedance component on heat exchanger performance. The results showed that Kapitza thermal conductivity results in a notable temperature gradient at the inlet, while axial thermal conductivity substantially diminishes the efficiency of the discrete heat exchanger. In the case of sintered heat exchangers, a geometric impedance component surpassing 4×10^{14} m^{-4} markedly influences both dimensionless temperature and pressure drop. Furthermore, in theoretical investigations of the holistic performance of dilution refrigeration cycles, the throttling process is commonly perceived as an isenthalpic expansion process. Zhai and Dang [5] investigated variations in specific cooling capacity, specific static heating power, and total cooling capacity concerning precooling temperature and upstream pressure at temperature of the mixing chamber of 10 mK. Furthermore, an in-depth analysis was conducted on the impact of primary heat exchanger efficiency on total cooling capacity. The results showed that, with a heat exchanger efficiency of 97%, the optimal upstream pressure and pre-cooling temperature were identified to be approximately 1.41×10^5 Pa and 4 K, respectively. Nevertheless, employing the isenthalpic expansion assumption for the throttling process in the two-phase region leads to inaccuracies. Li et al. [6] found that the average absolute deviation between the predicted natural gas temperature downstream of the impedance component using the isenthalpic expansion assumption and the test data was 2 K. Given the critical temperature of ^3He, which was merely 3.31 K, the temperature span within the two-phase region was even more limited

* Corresponding author at: State Key Laboratory of Infrared Physics, Shanghai Institute of Technical Physics, Chinese Academy of Sciences, 500 Yutian Road, Shanghai 200083, China.
E-mail address: haizheng.dang@mail.sitp.ac.cn (H. Dang).

https://doi.org/10.1016/j.cryogenics.2024.103832
Received 15 November 2023; Received in revised form 1 March 2024; Accepted 15 March 2024
Available online 16 March 2024

Nomenclature

CHEX	continuous heat exchanger
CFD	computational fluid dynamics
ρ_m	density of mixture
α_l	volume fraction of the liquid phase
ρ_l	density of liquid phase
$\mathbf{v}_l$	velocity vector of the liquid phase
$\mathbf{F}$	volume force
μ_l	vscosity of the liquid phase
k_{eff}	effective thermal conductivity
E_l	total energy of the liquid phase
h_l	enthalpy of the liquid phase
P	mixture pressure
v_v	velocity of the vapor phase
$m_{v,l}$	mass transport rates of condensation
T_l	liquid phase temperature
coeff_l	evaporation frequency, 1/s
m_l	mass flow rate of the outlet liquid, mg/s
m	mass flow rate of the mixture, mg/s
L_1	inlet tube length, mm
L_2	outlet tube length, mm
D_2	outlet diameter, mm
VF	volume fraction of ^{3}He liquid, %
T_{in}	inlet temperature, K
DHEX	discrete heat exchanger
$\mathbf{v}_m$	velocity vector of the mixture
α_v	volume fraction of the vapor phase
ρ_v	density of the vapor phase
$\mathbf{v}_v$	velocity vector of the vapor phase
μ_m	viscosity of the mixture
μ_v	viscosity of the vapor phase
S_E	volumetric heat source
E_v	total energy of the vapor phase
h_v	enthalpy of the vapor phase
T	mixture temperature
$m_{l,v}$	mass transport rates of evaporation
T_v	vapor phase temperature
T_{sat}	saturation temperature
coeff_v	condensation frequency, 1/s
m_v	mass flow rate of the outlet vapor, mg/s
L_r	liquefaction ratio, %
h	impedance component thickness, mm
D_1	inlet diameter, mm
D_3	impedance component diameter, mm
P_{in}	inlet pressure, kPa
P_{cr}	critical pressure, Pa

compared to that of natural gas [7]. Consequently, employing the isenthalpic expansion assumption for scrutinizing the throttling process of ^{3}He could result in noteworthy inaccuracies.

The computational fluid dynamics (CFD) is an effective method for predicting fluid-flow in the impedance component. Giacomelli [8,9] studied the flash evaporation of R744 through an ejector using a non-equilibrium evaporation condensation model, which can be applied to almost any type of compressible multiphase flow. Li et al. [10] developed a CFD throttling model of the CH_4–C_2H_6 binary mixture and discussed the condensation parameters of the CH_4–C_2H_6 binary mixture in the impedance component and Laval nozzle. Li et al. [11] used CFD modeling to establish the spontaneous condensation model of high-temperature and high-pressure condensed natural gas in the impedance component, analyzed the scouring effect of natural gas on the

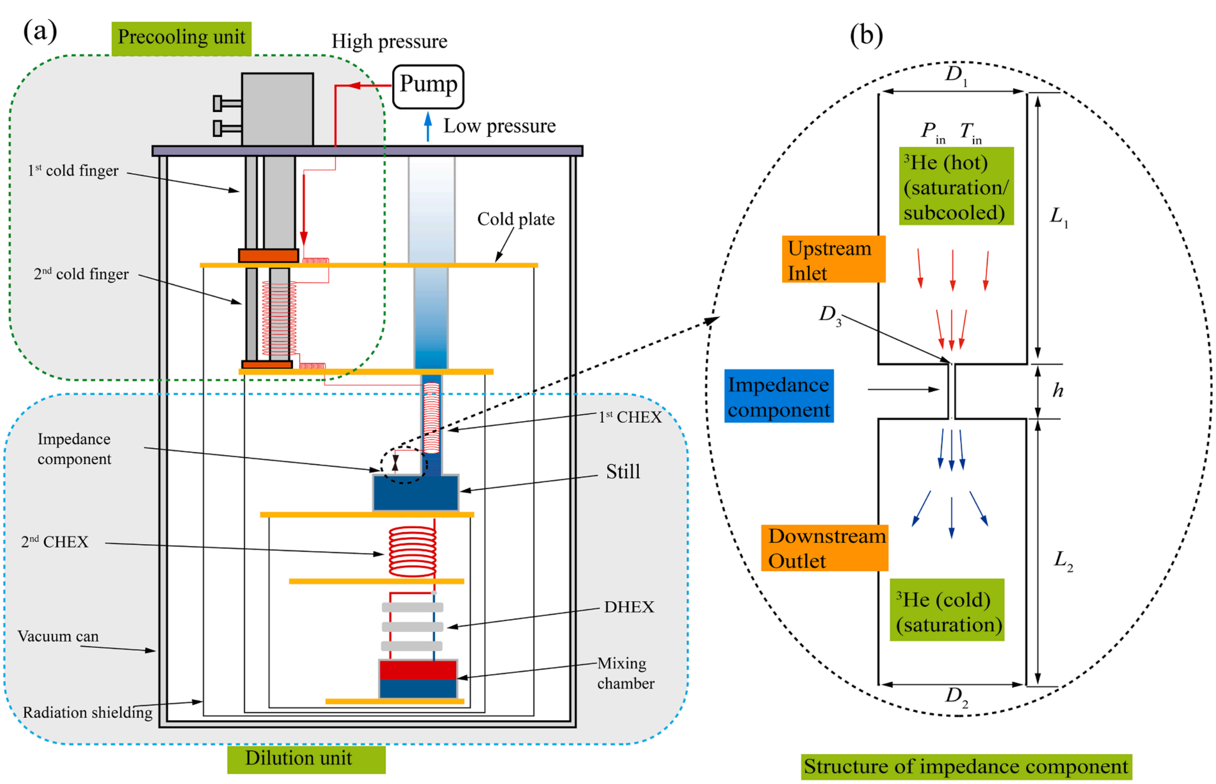

Fig. 1. Geometric model for simulation: (a) Dilution refrigeration cycle; (b) Structure of impedance component.

valve, and discussed the influence of condensation characteristics and latent condensation heat on the flow.

In the previous studies, most researchers focused on the performance of heat exchangers, with little attention paid to the influence of the impedance component on the performance of dilution refrigerators. In addition, the method based on the isenthalpic expansion assumption was unsuitable for studying the influencing factors of impedance component throttling performance in the two-phase region, and the error would become more significant as the critical temperature of the material decreased. The CFD method has become an effective approach to analyzing the influencing factors of impedance component throttling performance due to its accuracy and high efficiency. However, it is rarely used to analyze the throttling process of liquid ^{3}He. Therefore, a numerical model was developed to clarify the energy conversion mechanism during the throttling process of liquid ^{3}He and improve the ^{3}He liquefaction by optimizing work conditions.

2. Numerical model

2.1. Geometric model

Fig. 1 (a) illustrates the configuration of a dilution refrigerator, comprising a pre-cooling unit, a dilution refrigeration unit, a pump unit, and other components. Following precooling by the precooling unit, ^{3}He achieves a lower temperature via the impedance component in the dilution unit. Subsequently, it undergoes heat exchange through still, continuous heat exchanger, and discrete heat exchangers. Upon reaching the mixing chamber, it traverses the phase interface, resulting in the generation of cooling capacity. Fig. 1 (b) illustrates the geometric model of the impedance component. The inlet tube length (L_1), impedance component thickness (h), outlet tube length (L_2), inlet diameter (D_1), outlet diameter (D_2) and impedance component diameter (D_3) are 5 mm, 0.4 mm, 10 mm, 2.0 mm, 2.0 mm and 0.02 mm, respectively.

2.2. The state of ^{3}He

The investigation of the throttling process of ^{3}He necessitates dedicate distinctions among its various states. Inspired by the methodology used for differentiating substance states in water [12], the material states of ^{3}He have been finely categorized, and the physical property data for ^{3}He is obtained from Ref. [13]. Fig. 2 (a) visually represents the distribution of ^{3}He states on the T-S diagram, while Fig. 2 (b) provides a graphical representation of the state distribution on the P-T diagram. In the range between saturation pressure and critical pressure, the substance assumes a subcooled liquid state, resembling an incompressible liquid. Beyond the critical pressure, it transitions into a compressible liquid state. Within this compressible liquid range, temperatures surpassing the critical temperature mark the substance's behavior as that of a critical fluid. By projecting a tangent line backward from the critical point, the critical fluid can be discerned into distinct liquid and vapor phases.

2.3. Mathematical model

Several necessary assumptions were made in the mathematic model for the throttling process of ^{3}He: (1) The steady-state model is used; (2) The gas radiation is not considered; (3) The influence of gravity is not considered; The mass, momentum, energy, and species conservation equations are given as follows, respectively:

Continuity equations:

$$\nabla\cdot(\rho_m \mathbf{v}_m) = 0 \tag{1}$$

$$\rho_m = \alpha_l\rho_l + \alpha_v\rho_v \tag{2}$$

$$\mathbf{v}_m = \frac{\alpha_l\rho_l\mathbf{v}_l + \alpha_v\rho_v\mathbf{v}_v}{\rho_m} \tag{3}$$

Momentum equations:

$$\nabla\cdot(\rho_m\mathbf{v}_m\mathbf{v}_m) = -\nabla p + \nabla\cdot\left[\mu_m\left(\nabla\mathbf{v}_m + \nabla\mathbf{v}_m^{\mathrm{T}}\right)\right] + \mathbf{F} \tag{4}$$

$$\mu_m = \alpha_l\mu_l + \alpha_v\mu_v \tag{5}$$

Energy equations:

$$\nabla\cdot[\alpha_l\mathbf{v}_l(\rho_l E_l + p) + \alpha_v\mathbf{v}_v(\rho_v E_v + p)] = \nabla\cdot(k_{eff}\nabla T) + S_E \tag{6}$$

$$E_l = h_l - \frac{p}{\rho_l} + \frac{v_l^2}{2} \tag{7}$$

$$E_v = h_v - \frac{p}{\rho_v} + \frac{v_v^2}{2} \tag{8}$$

Vapor mass fraction equations:

$$\nabla\cdot(\alpha_v\rho_v\mathbf{v}_v) = m_{l,v} - m_{v,l} \tag{9}$$

The Lee phase transition model as follows [14]:
Mass transfer from liquid phase to vapor phase:

$$m_{l,v} = \mathrm{coeff}_l\cdot\alpha_l\rho_l\frac{T_l - T_{sat}}{T_{sat}} \tag{10}$$

Mass transfer from vapor phase to liquid phase:

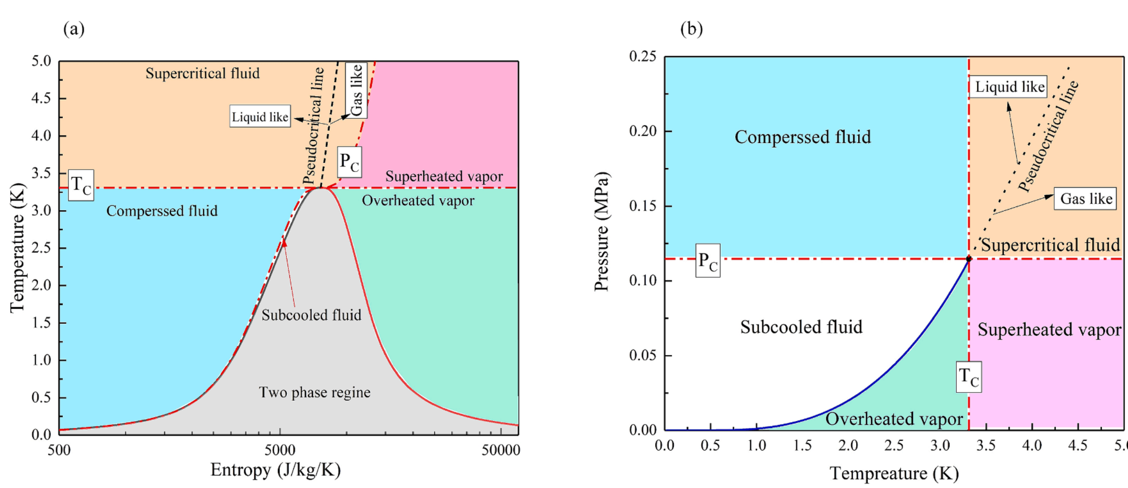

Fig. 2. The state of ^{3}He: (a) State distribution on T-S diagram; (b) State distribution on P-T diagram.

$$m_{\mathrm{v,l}} = \mathrm{coeff}_{\mathrm{v}} \cdot \alpha_{\mathrm{v}} \rho_{\mathrm{v}} \frac{T_{\mathrm{v}} - T_{\mathrm{sat}}}{T_{\mathrm{sat}}} \tag{11}$$

where ρ_{m} is the density of the mixture; $\mathbf{v}_{\mathrm{m}}$ the velocity vector of mixture; α_{l}, ρ_{l}, $\mathbf{v}_{\mathrm{l}}$ the volume fraction, density and velocity vector of liquid phase, respectively; α_{v}, ρ_{v}, $\mathbf{v}_{\mathrm{v}}$ the volume fraction, density and velocity vector of vapor phase, respectively; $\mathbf{F}$ the volume force; μ_{m}, μ_{l}, μ_{v} the viscosity of the mixture, the liquid phase and the vapor phase, respectively;k_{eff} the effective thermal conductivity; S_E the volumetric heat source; P the pressure of mixture; T the temperature of mixture; E_{l}, E_{v} the total energy of the liquid phase and the vapor phase; h_{l}, h_{v} the enthalpy of the liquid phase and the vapor phase; v_{v} the velocity of vapor phase; $m_{\mathrm{l,v}}$ and $m_{\mathrm{v,l}}$ the mass transport rates of evaporation and condensation, respectively; T_{v}, T_{l}, T_{sat} the vapor phase temperature, liquid phase temperature and saturation temperature, respectively; $\mathrm{coeff}_{\mathrm{l}}$, $\mathrm{coeff}_{\mathrm{v}}$ the evaporation and condensation frequency.

The Lee phase transition model has been modified to meet the conditions of subcooling to saturation, as shown in Fig. 3:

(1) Comparing P with P_{cr} to determine the state of ^{3}He;

(2) $\mathrm{coeff}_{\mathrm{l}}$/ $\mathrm{coeff}_{\mathrm{v}}$ = saturation liquid density/saturation vapor density, and $\mathrm{coeff}_{\mathrm{v}} = 1$ 1/s [15];

(3) The density of the vapor and liquid phases is determined by P, T_{v}, and P, T_{l}, respectively;

(4) The P-T relationship formula in the saturated state determines the saturation temperature T_{sat}, i.e. $T_{\mathrm{sat}}=f(P)$.

The liquefaction ratio in downstream is expressed as:

$$Lr = \frac{m_{\mathrm{l}}}{m_{\mathrm{l}} + m_{\mathrm{v}}} \times 100\% = \frac{m_{\mathrm{l}}}{m} \times 100\% \tag{12}$$

where m_{l} is the mass flow rate of outlet liquid, m_{v} is the mass flow rate of outlet vapor, m is the mass flow rate of mixture.

2.4. Computational model

The simulation employed the SST k-ω turbulence model to address low-velocity turbulence [16–18]. The mixture model was selected to solve the multiphase flow. A User Defined Function (UDF) has been developed to describe interphase mass transfer at different saturation temperatures. A real physical property model has been built in 1.5-2.5 K: various complex physical properties are embedded in UDF in an array form, and physical properties can be accurately determined through temperature and pressure. Various physical property data such as specific heat, density, local sound speed, viscosity, thermal conductivity, enthalpy and latent heat in the UDF were calculated by Huang et al. [7,19–23]. Convergence criteria were set at 1×10^{-5} for continuity, momentum, and species, while the energy residual standard was established at 1×10^{-8}. The steady flow was addressed using a pressure-velocity coupling algorithm. The discretization schemes for pressure and volume fraction were specified as Body Force Weighted and QUICK, respectively, with others configured as Second-Order Upwind. This model has been successfully applied to ^{4}He throttling in our laboratory and experimentally verified [24].

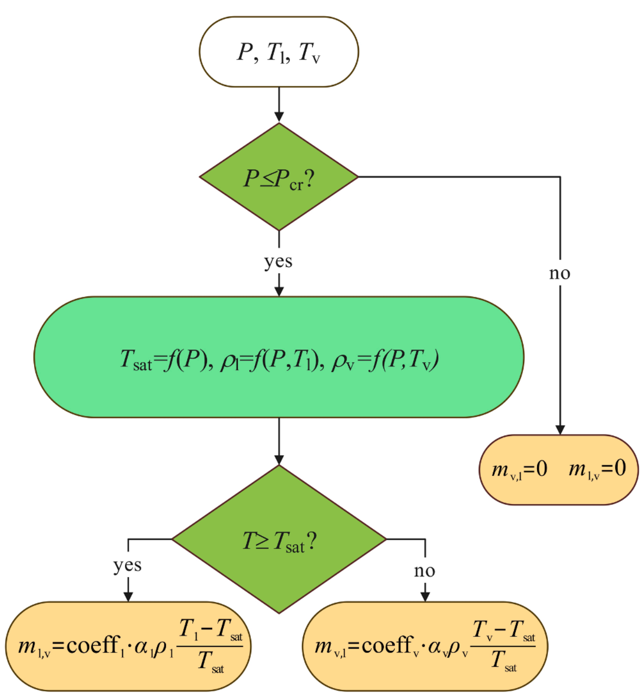

Fig. 3. Schematic diagram of the improved Lee phase transition model.

The following boundary conditions were applied in the numerical model: (1) The inlet is a pressure inlet with a total pressure of 44.01 kPa (2.5 K saturation pressure), 60.00 kPa, 80.00 kPa and an initial gauge pressure of 44.01 kPa, 60.00 kPa, 80.00 kPa since the inlet speed is very small with a turbulence intensity of 0%; (2) The inlet temperature is 2.0 K, 2.3 K, 3 K; (3) The outlet is a pressure outlet boundary with a gauge pressure of 6.7098 kPa (1.5 K saturation temperature), a turbulence intensity of 5% and a reflow gas volume fraction of 0; (4) The side wall is adiabatic.

The CFD method requires discretizing the simulation area into small control units, i.e. dividing the grid. Considering the calculation time and accuracy, only half of the structure is grided, and a structured grid of impedance component in 2D is established, as shown in Fig. 4. Considering the influence of the boundary layer on the results, the boundary layer is refined. If the number of grids divided is small, it will impact the calculation results. Therefore, the independence of the grids has been verified.. In other words, when the final number of grids is increased to 169,000, its effect on the calculation results is negligible. Therefore, the number of grids selected for the simulation unit is 169,000.

3. Results and discussions

3.1. Effect of inlet pressure on throttling performance

Fig. 5 illustrates the temperature and volume fraction (VF) of ^{3}He liquid near the impedance component under the conditions of a 2.5 K inlet temperature, 1.5 K refrigeration temperature, and 60 kPa inlet pressure. The contour shows that supercooled or saturated liquid undergoes phase change downstream after being depressurized by an impedance component and is cooled by latent heat. It is worth emphasizing that phase change only occurs downstream, and there is no phase change inside the impedance component, which becomes the boundary of phase change. For the process of liquid throttling to the 2-phase state, the pressure after throttling is entirely determined by the back pressure. In contrast, in the single-phase condition before and after throttling, the pressure after throttling is not necessarily determined by the back pressure. The energy change during the single-phase throttling process that is, the cooling or heating after throttling, entirely depends on the change in enthalpy value. When a single-phase liquid is throttled to the 2-phase state, the temperature must decrease after throttling, and the cooling amount comes from the latent heat of phase change. For the impedance component of the orifice structure, the throttling process of liquids is similar to jetting, and the phase change occurs outside the impedance component. For the impedance component of the wire-in-tube structure, the throttling process of the liquid is similar to boiling inside the tube, and the phase change occurs inside the impedance component.

Fig. 6 shows the pressure and velocity contours near the impedance component at 44.01 kPa (saturation pressure at 2.5 K), 60.00 kPa, 80.00 kPa inlet pressure, a 2.5 K inlet temperature, and a 1.5 K refrigeration temperature. There is a low-pressure area near the inlet of the

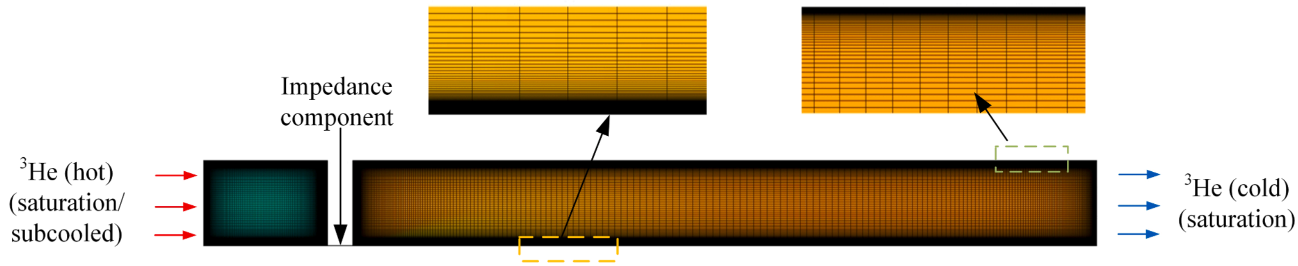

Fig. 4. Grid of simulation unit.

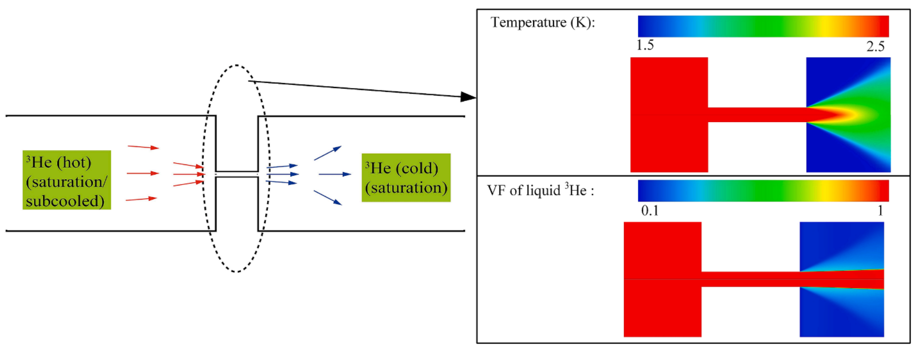

Fig. 5. The contours of temperature and VF near the impedance component.

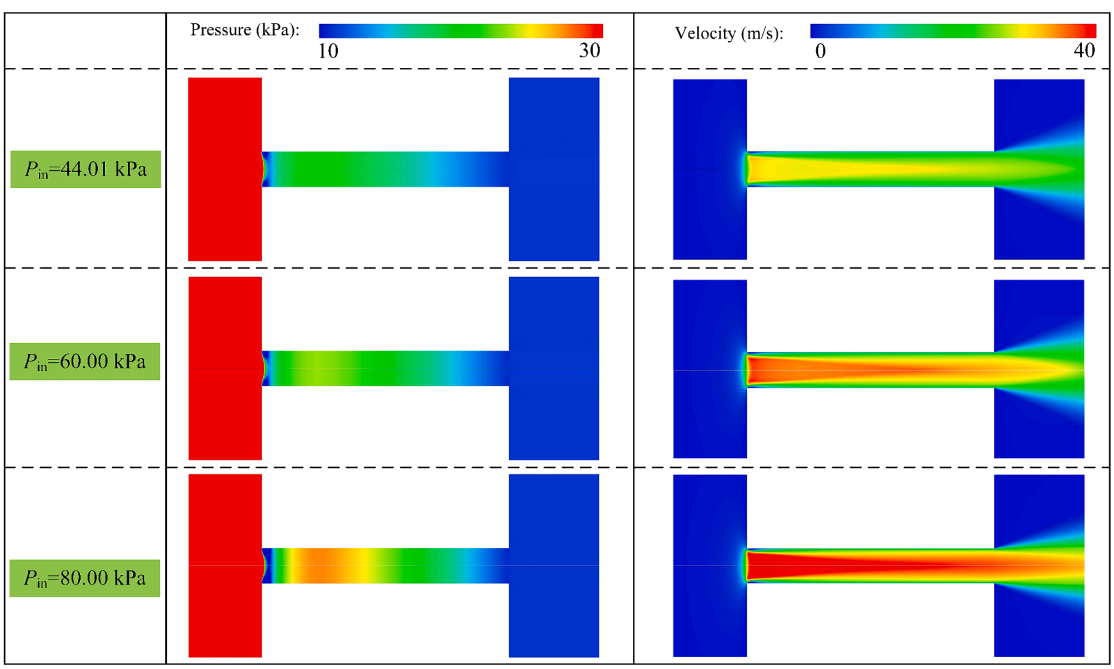

Fig. 6. The contours of pressure and velocity inside and outside of the impedance for different inlet pressures.

impedance component, which is caused by a sudden and rapid increase in velocity. The velocity converges towards the centerline, so there is the lowest pressure near the wall. As the inlet pressure increases, the inlet velocity of the impedance component increases, and the area of the low-pressure area increases. The impedance component exhibits a pressure distribution of decreasing, increasing, and then decreasing. At an inlet pressure of 80 kPa, there is an area close to 30 kPa, which is caused by a large amount of dynamic pressure converting into static pressure. The speed is significantly affected by the inlet pressure. As the inlet pressure increases, the maximum speed inside the impedance component increases and the average speed increases.

Fig. 7 shows the mass flow rate and liquefaction ratio of 3He under the inlet pressures of 44.01 kPa (saturation pressure at 2.5 K), 60.00 kPa, 80.00 kPa, respectively, at the inlet temperature of 2.5 K and the refrigeration temperature of 1.5 K, which is essential in the design of dilution refrigerators. As the pressure increases, the mass flow rate increases. An impedance component with a diameter of 0.02 mm will achieve a flow rate of 0.74 mg/s at 80 kPa. Fig. 7 (b) shows the liquefaction ratios of a real and under the assumption of isenthalpic expansion. The liquefaction ratio of the real throttling process is more

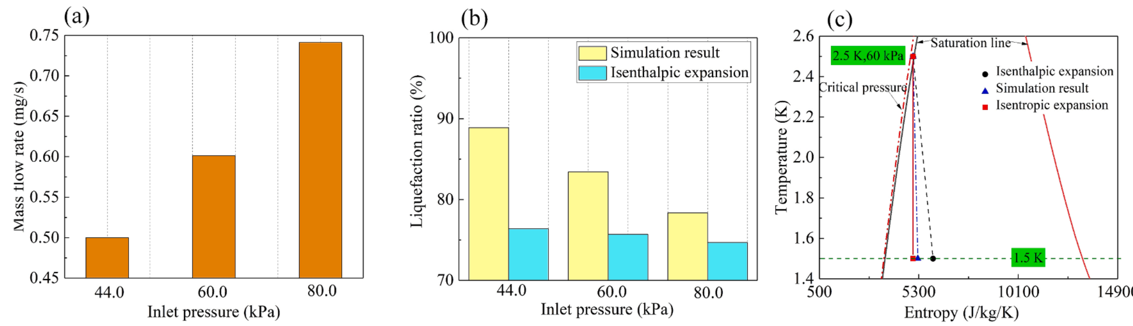

Fig. 7. Refrigeration performance under different inlet pressure: (a) Mass flow rate; (b) Liquefaction ratio of ^{3}He; (c) Isentropic expansion, isenthalpic expansion, and simulation result on T-S diagram.

significant than that under the assumption of isenthalpic expansion. The liquefaction ratio decreases with the increasing pressure. This is attributed to the surge in pressure, causing a subsequent augmentation in downstream total energy, heightened consumption of latent heat, a reduction in the quantity of liquid downstream, and, ultimately, a diminished liquefaction ratio. Fig.7 (c) shows the isentropic expansion process, isenthalpic expansion process, and the simulation results of throttling from 2.5 K and 60 kPa to 1.5 K on the T-S diagram. The real throttling process is between the isenthalpic and isentropic expansion processes. Combined with the variation law of liquefaction ratio, at 80 kPa, the real throttling process is closer to the isenthalpic one (with a smaller difference in liquefaction ratio compared to the isenthalpic expansion process). At 40.01 kPa, the actual throttling process is closer to the isentropic expansion one (with a greater difference in liquefaction ratio compared to the isenthalpic expansion process). From the perspective of improving throttling efficiency, it is best to be in a saturated state before throttling.

3.2. Effect of inlet temperatures on throttling performance

Fig. 8 presents pressure and velocity contours under varying inlet temperatures (2.0 K, 2.2 K, 2.5 K) with a fixed inlet pressure of 60 kPa and refrigeration temperature of 1.5 K. The inlet temperature significantly impacts the pressure inside the impedance component. As the temperature increases, the pressure inside the impedance component increases, which is attributed to changes in density. Specifically, higher temperatures correspond to lower densities. At a constant total pressure, this will result in a decrease in dynamic pressure and an increase in static pressure.

Fig. 9 shows the ^{3}He mass flow rate and liquefaction ratio under varying inlet temperatures (2.0 K, 2.2 K, 2.5 K) with a fixed inlet pressure of 60 kPa and a refrigeration temperature of 1.5 K. The temperature change has little effect on the mass flow rate, with an inlet temperature change of 0.5 K and a flow rate of only 0.05 mg/s. This is related to the density ^{3}He at low temperatures, which decreased from 2.5 K to 2 K, with a density change of only 5.3 kg/m^3. The liquefaction ratio decreases with the increase of inlet temperature, and the real liquefaction ratio is significantly higher than that under the assumption of isenthalpic expansion. This is because the lower the temperature, the more significant the latent heat, the less liquid consumed during phase change, and the higher the liquefaction ratio.

4. Conclusions

As one of the key components of the dilution refrigerator, the impedance component is used to control the flow and to liquefy ^{3}He, which is crucial to achieving millikelvin temperature. A numerical study was performed in this work to study the energy conversion on the throttling process and effects of the inlet pressure and inlet temperature on the flow rate and liquefaction ratio. The following important

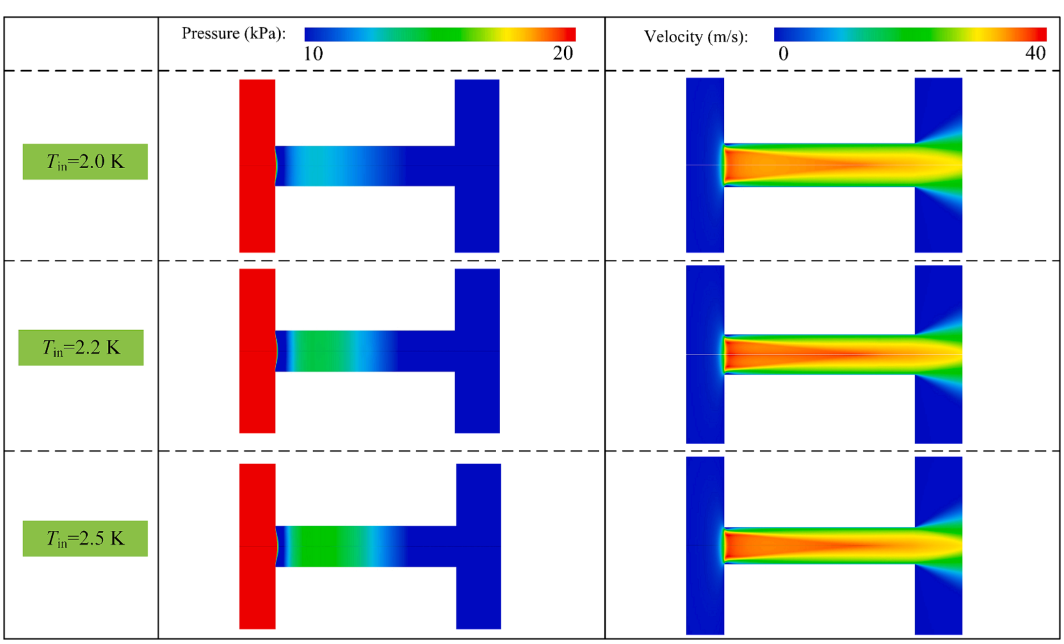

Fig. 8. The contours of pressure and velocity near the impedance component under different inlet temperatures.

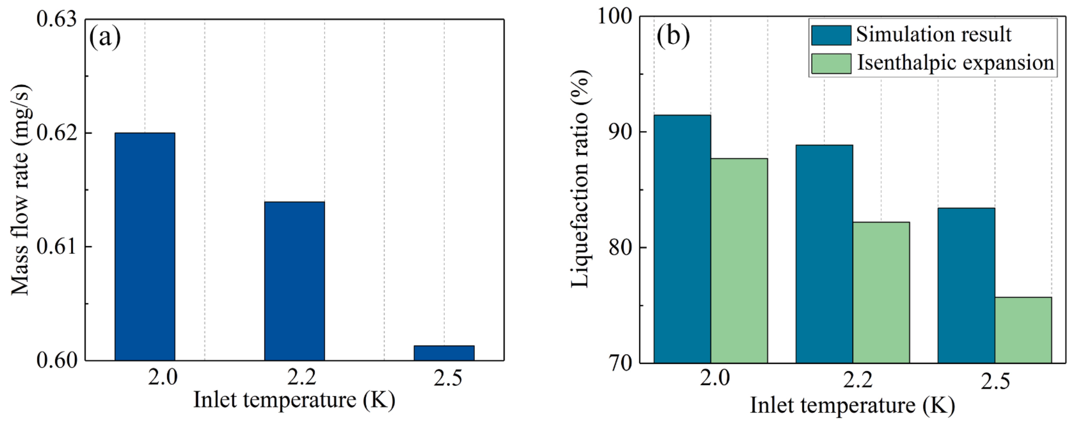

Fig. 9. Refrigeration performance under different inlet temperatures: (a) Mass flow rate; (b) Liquefaction ratio of ^{3}He.

conclusions are obtained:

(1) For liquid throttling to a two-phase state, the pressure after throttling is only determined by the back pressure, and the phase change only occurs in downstream, cooling itself through latent heat.

(2) The flow rate increases with the decreasing temperature and the increasing pressure. Inlet temperature has little effect on flow rate, with an increase of 0.5 K in temperature and only a change of 0.05 mg/s in flow rate.

(3) The liquefaction ratio increases with the decreasing temperature or pressure. The difference in liquefaction ratio between the simulation result and the isenthalpic expansion process decreases with the decreasing temperature or the increasing pressure.

(4) There is a certain deviation between the throttling process under the assumption of isenthalpic expansion and the real throttling process, so the assumption of isenthalpic expansion cannot be used to solve throttling problems at ultralow temperatures.

CRediT authorship contribution statement

Shiguang Wu: Conceptualization, Data curation, Investigation, Methodology, Writing – original draft. **Haizheng Dang:** Conceptualization, Funding acquisition, Investigation, Methodology, Supervision, Writing – original draft, Writing – review & editing.

Declaration of competing interest

The authors declare that they have no known competing financial interests or personal relationships that could have appeared to influence the work reported in this paper.

Data availability

Data will be made available on request.

Acknowledgements

This work is supported by the National Natural Science Foundation of China (Grant No. 52076210), the Major Project of Science and Technology Commission of Shanghai Municipality (Grant No. 22511100100), the Collaborative Innovation Project of Shanghai Municipality (Grant No. XTCX-KJ-2023-58) and Shanghai Municipal Science and Technology Major Project (Grant No. 2019SHZDZX01).

References

[1] Korzh B, Zhao Q-Y, Allmaras JP, Frasca S, Autry TM, Bersin EA, et al. Demonstration of sub-3 ps temporal resolution with a superconducting nanowire single-photon detector. Nature Photon 2020;14(4):250–5. https://doi.org/10.1038/s41566-020-0589-x.

[2] Zhong HS, Wang H, Deng YH, Chen MC, Peng LC, Luo YH, et al. Quantum computational advantage using photons. Science 2020;370(6523):1460–3. https://doi.org/10.1126/science.abe8770.

[3] Zu H, Dai W, de Waele ATAM. Development of dilution refrigerators—a review. Cryogenics. 2022;121. https://doi.org/10.1016/J.cryogenics.2021.103390.

[4] Shang XS, Miao Z, Cao HQ, Wang R, Shao W, Cui Z. Modeling on cryogenic heat exchangers considering variable properties, axial heat conduction and viscous heating. Int J Refrigerat 2023;146:381–9. https://doi.org/10.1016/j.ijrefrig.2022.11.028.

[5] Zhai Y, Dang H. Performance optimization of a mK dilution refrigerator based on the first law of thermodynamics. Cryogenics 2023;135. https://doi.org/10.1016/j.cryogenics.2023.103731.

[6] Li C, Jia W, Wu X. Temperature prediction for high pressure high temperature condensate gas flow through chokes. Energies. 2012;5(3):670–82. https://doi.org/10.3390/en5030670.

[7] Huang Y, Chen G, Arp V. Debye equation of state for fluid helium-3. J Chem Phys. 2006;125(5):054505. https://doi.org/10.1063/1.2217010.

[8] Giacomelli F, Mazzelli F, Milazzo A. A novel CFD approach for the computation of R744 flashing nozzles in compressible and metastable conditions. Energy. 2018; 162:1092–105. https://doi.org/10.1016/j.energy.2018.08.050.

[9] Giacomelli F, Mazzelli F, Banasiak K, Hafner A, Milazzo A. Experimental and computational analysis of a R744 flashing ejector. Int J Refrigerat 2019;107: 326–43. https://doi.org/10.1016/j.ijrefrig.2019.08.007.

[10] Li C, Zhang C, Li Z, Jia W. Numerical study on the condensation characteristics of natural gas in the throttle valve. J Natural Gas Sci Eng 2022;104. https://doi.org/10.1016/j.jngse.2022.104689.

[11] Li Z, Zhang C, Li C, Jia W. Thermodynamic study on the natural gas condensation in the throttle valve for the efficiency of the natural gas transport system. Appl Energy 2022;322. https://doi.org/10.1016/j.apenergy.2022.119506.

[12] Mokry S, Pioro I, Farah A, King K, Gupta S, Peiman W, et al. Development of supercritical water heat-transfer correlation for vertical bare tubes. Nucl Eng Des 2011;241(4):1126–36. https://doi.org/10.1016/j.nucengdes.2010.06.012.

[13] Huang Y, Chen G, Arp V. Helium-3 Thermophysical Properties Program – He3Pak, Version2.0. Shanghai Jiao Tong University, 2009. (available from Horizon Technologies, Littleton, CO, USA, https://htess.com.).

[14] Lee WH. Pressure iteration scheme for two-phase flow modeling. IN“ MULTIPHASE TRANSPORT: FUNDAMENTALS, REACTOR SAFETY, APPLICATIONS”. 1980407-32.

[15] Czerwiński G, Wołoszyn J. Numerical study of a cooling system using phase change of a refrigerant in a thermosyphon. Energies 2021;14(12). https://doi.org/10.3390/en14123634.

[16] Mazzelli F, Little AB, Garimella S, Bartosiewicz Y. Computational and experimental analysis of supersonic air ejector: turbulence modeling and assessment of 3D effects. Int J Heat Fluid Flow. 2015;56:305–16. https://doi.org/10.1016/j.ijheatfluidflow.2015.08.003.

[17] Teng L, Liu X, Bian J, Li Y, Lu C. A homogeneous relaxation model for multi-phase CO_2 jets following the release of supercritical CO_2 pipelines. J Nat Gas Sci Eng 2020;84. https://doi.org/10.1016/j.jngse.2020.103609.

[18] Haida M, Smolka J, Hafner A, Palacz M, Banasiak K, Nowak AJ. Modified homogeneous relaxation model for the R744 trans-critical flow in a two-phase ejector. Int J Refrigerat 2018;85:314–33. https://doi.org/10.1016/j.ijrefrig.2017.10.010.

[19] Huang Y, Chen G. Melting-pressure and density equations of He 3 at temperatures from 0.001 to 30 K. Phy Rev B. 2005. https://doi.org/10.1103/PhysRevB.72.184513.

[20] Huang Y, Chen G, Li X, Arp V. Density equation for saturated ^{3}He. Int J Thermophys 2005;26:729–41. https://doi.org/10.1007/s10765-005-5574-6.

[21] Huang Y, Chen G. A practical vapor pressure equation for helium-3 from 0.01 K to the critical point. Cryogenics. 2006;46(12):833–9. https://doi.org/10.1016/j.cryogenics.2006.07.006.

[22] Huang Y, Fang L, Wang X, Wang R, Xu L. Thermal conductivity of helium-3 between 3 mK and 300 K. In: AIP Conference Proceedings. American Institute of Physics; 2012. p. 1849–56. https://doi.org/10.1063/1.4707122.
[23] Huang Y, Yu Q, Chen Q, Wang R. Viscosity of liquid and gaseous helium-3 from 3 mK to 500 K. Cryogenics. 2012;52(10):538–43. https://doi.org/10.1016/j.cryogenics.2012.06.011.
[24] Wu S, Zhao B, Tan J, Zhao Y, Zhai Y, Xue R, et al. Thermodynamic study on throttling process of Joule-Thomson cooler to improve helium liquefaction performance between 2 K and 4 K. Energy 2023;277. https://doi.org/10.1016/j.energy.2023.127691.